Nanoscale Res Lett (2006) 1:1–10
DOI 10.1007/s11671-006-9014-8

NANO REVIEW

Multi-scale ordering of self-assembled InAs/GaAs(001) quantum dots

S. Kiravittaya · R. Songmuang · A. Rastelli · H. Heidemeyer · O. G. Schmidt

Published online: 25 July 2006

Abstract Ordering phenomena related to the self-assembly of InAs quantum dots (QD) grown on GaAs(001) substrates are experimentally investigated on different length scales. On the shortest length-scale studied here, we examine the QD morphology and observe two types of QD shapes, i.e., pyramids and domes. Pyramids are elongated along the [1–10] directions and are bounded by {137} facets, while domes have a multi-facetted shape. By changing the growth rates, we are able to control the size and size homogeneity of freestanding QDs. QDs grown by using low growth rate are characterized by larger sizes and a narrower size distribution. The homogeneity of buried QDs is measured by photoluminescence spectroscopy and can be improved by low temperature overgrowth. The overgrowth induces the formation of nanostructures on the surface. The fabrication of self-assembled nanoholes, which are used as a template to induce short-range positioning of QDs, is also investigated. The growth of closely spaced QDs (QD molecules) containing 2–6 QDs per QD molecule is discussed. Finally, the long-range positioning of self-assembled QDs, which can be achieved by the growth on patterned substrates, is demonstrated. Lateral QD replication observed during growth of three-dimensional QD crystals is reported.

Keywords Self-assembly · Semiconductor quantum dots · Photoluminescence

S. Kiravittaya (✉) · R. Songmuang · A. Rastelli · H. Heidemeyer · O. G. Schmidt
Max-Planck-Institut für Festkörperforschung, Heisenbergstrasse 1, D-70569 Stuttgart, Germany
e-mail: s.kiravittaya@fkf.mpg.de

Introduction

Over the last decade semiconductor quantum dots (QDs) have attained much interest due to their electronic properties characterized by discrete atomic-like energy levels [1, 2]. Nowadays, self-assembled QDs are widely used as a playground to study novel physical phenomena such as cavity quantum electrodynamics [3, 4], as well as building blocks for high performance QD-based devices [1, 5]. In general, understanding the formation and evolution of self-assembled QDs on any specific length scale is required in order to fully engineer the QD structures.

Recently, several concepts on the ordering of self-assembled QD systems on different length scales have been proposed and demonstrated [6–8]. With reference to Fig. 1, we can describe the route towards ordering of self-assembled QDs at different length scales. At the shortest length scale, we consider the ordering at the level of individual QDs, which can be sub-divided into ordering in shape, size, and composition. The QD shape can be ordered under certain conditions, i.e., a monomodal distribution of QD shapes can be obtained. The formation, evolution and shape transitions are also discussed in this context. We can improve QD size and composition homogeneity by changing the QD growth conditions. The QD overgrowth procedure plays also an important role in determining the degree of order. The concept of order can be extended to the spatial arrangement of QDs. Groups of closely spaced QDs, termed lateral QD molecules, can be obtained by means of an in situ etching technique. The etching produces self-assembled nanoholes which can be used as a template to guide the formation of QD molecules. The longest length scale of ordering in self-assembled

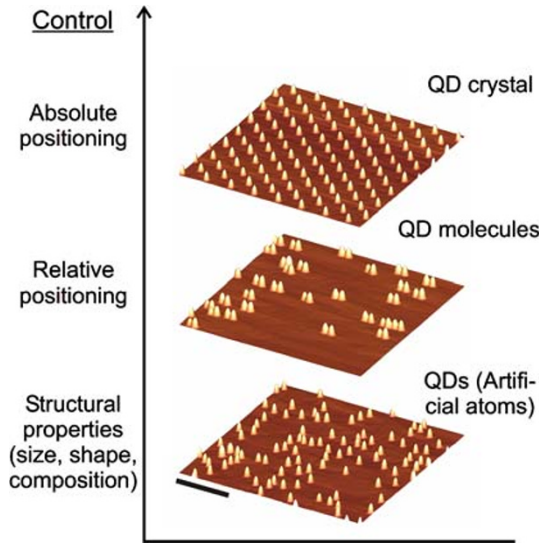

Fig. 1 Route towards controlling the ordering of self-assembled QD structures. Scale bar corresponds to 500 nm

QDs is the absolute positioning. This can be achieved by growing QDs on patterned substrates.

In this paper, we will present a route to achieve QD ordering on multiple length scales. The experimental observations are based on the self-assembled InAs/GaAs QD system. The route starts with the shape of freestanding QDs, followed by the homogeneity of buried QDs. The local QD positioning and the fabrication of short-range ordered QDs (QD molecules) are also reported. Finally, we briefly present our recent results on the long-range positioning of self-assembled QDs on patterned substrates.

QD shapes

The surface morphology of InAs QDs grown on GaAs(001) has received relatively little attention compared to the QD electronic and optical properties. This is mainly due to the nanometric size of the QDs, which renders it difficult to obtain detailed information from commonly used atomic force microscopy (AFM). Under usual growth conditions, the QD surface is bounded by well-defined crystal planes. By taking advantage of the high resolution of scanning tunneling microscopy (STM), Márquez et al. [9] have identified the facets composing the surface of small QDs as {137}. By using reflection high-energy electron diffraction (RHEED) [10], transmission electron microscopy (TEM) [11], and STM [12], steep facets, such as {101}, have been observed on the surface of larger QDs. The detailed shape of such QDs has been revealed by a facet analysis of STM data [13, 14], allowing to draw a coherent picture describing the QD morphology. Similarly to the well-characterized SiGe/Si(001) material system [8, 15], two facetted morphologies have been identified: small and shallow {137}-facetted pyramids and larger multi-facetted domes.

Figure 2a shows a three-dimensional (3D) view of an STM image of InAs QDs on a flat GaAs(001) surface [12]. The QDs are grown by a solid-source molecular beam epitaxy system at a low growth rate of 0.01 monolayers/s (ML/s) and a relatively high substrate temperature (500 °C). From this measurement we observe small elongated InAs pyramids and large multi-facetted domes [12]. A schematic picture of pyramidal QDs is shown in Fig. 2b. As one clearly sees from the STM image (Fig. 2a), the dome-shaped QDs are much larger than the pyramid-shaped QDs. In agreement with previous reports [16] and with what is observed in the SiGe system [17], we believe that a morphological transition occurs from pyramid to dome shape when the amount of deposited material is increased or the system ripens during in situ annealing. The analysis of the dome shape reveals several facet planes. The facets with largest area have {101} indices. Smaller {111} facets are also observed at the QD base. The {137} facets are still observed at the top and bottom of the dome, indicating that during the shape transition, steep facets form and expand while the {137} facets shrink. A schematic representation of a dome-shaped QD is shown in Fig. 2c. On the atomic-scale, the surface reconstruction of the {137} facets was reported in Ref. [9]. The (1×1)-reconstructed {101}

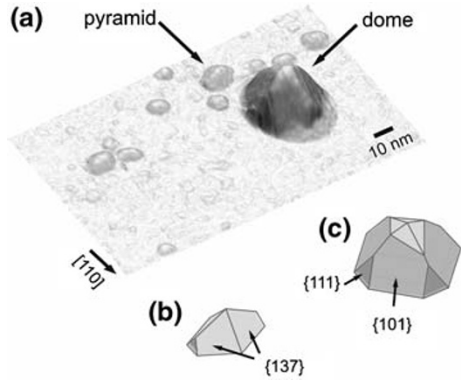

Fig. 2 (**a**) 3D view STM image of pyramid-shaped and dome-shaped InAs QDs on a flat GaAs(001) surface. Schematic representation of (**b**) a pyramid and (**c**) a dome. Data courtesy of C. Manzano, G. Costantini, Nanoscale Science Department, Max-Planck-Institute Stuttgart

facets and the (2 × 2)-reconstructed {111} facets of the domes were studied in Ref. [13].

Ordering in QD size

Free-standing QDs

The size fluctuation of self-assembled QDs grown under typical growth conditions is about ±10% [18]. However, the size homogeneity can be improved by optimizing the growth conditions [6]. Figure 3 shows the histogram of the height distribution of InAs QDs grown at 500 °C using different growth rates. The 3D AFM images of QDs on the surface are shown in the insets. We clearly see that the lower growth rate induces larger QDs with better size homogeneity [6, 19]. We can explain this effect by different migration lengths of In adatoms [20]. At a low growth rate (large migration length), the In adatoms are preferentially incorporated into existing QDs, rather than forming new QDs. The long migration length produces also a better size homogeneity of the QD array. This can be explained by the fact that when In adatoms can migrate longer, they have a higher chance of finding a lower energy position to be incorporated. Since larger QDs produce higher strain barriers, the In adatoms prefer to incorporate into smaller QDs. Such an effect is called self-limiting growth [21].

For general electronic and optical applications, burying the QDs in higher band gap material is of interest. Photoluminescence (PL) spectroscopy is a typical tool for the investigation of the buried QD structure. Figure 4 shows room temperature PL spectra obtained from QDs, which were grown under the same growth conditions as the QDs shown in Fig. 3, but were overgrown with GaAs layers. The PL linewidth obtained from a QD ensemble is generally attributed to the inhomogeneous broadening produced by the size and composition fluctuations of the QDs in the ensemble. The variation of the PL linewidth as well as the PL peak energy are well consistent with the QD size and size distribution observed by AFM, i.e., the larger QDs with narrower size distribution provide longer wavelength emission with narrower emission linewidth [19, 20, 22].

Buried QDs

The size, shape, and composition of QDs in an array are affected not only by the QD growth conditions but also by the overgrowth conditions. The influence of the substrate temperature during GaAs overgrowth has been investigated by PL spectroscopy [19, 22]. Figure 5 shows room temperature PL spectra of 1.8 ML InAs

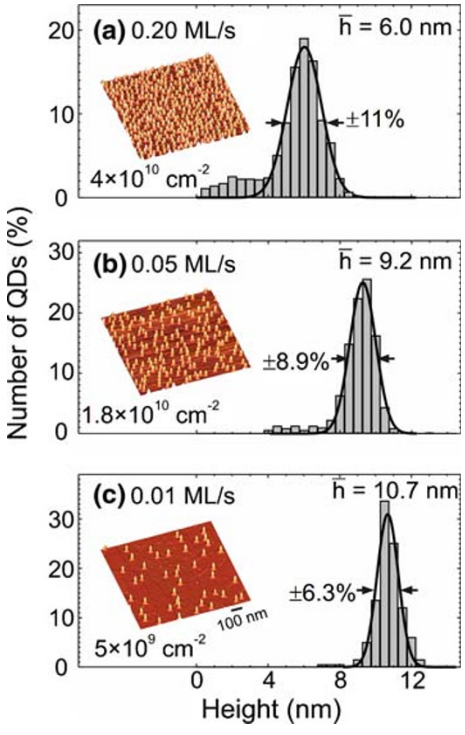

Fig. 3 Height histograms of 1.8 ML InAs QDs grown at different InAs growth rates of (**a**) 0.01 ML/s, (**b**) 0.05 ML/s, and (**c**) 0.2 ML/s. Insets show the corresponding 1 × 1 μm^2 AFM images

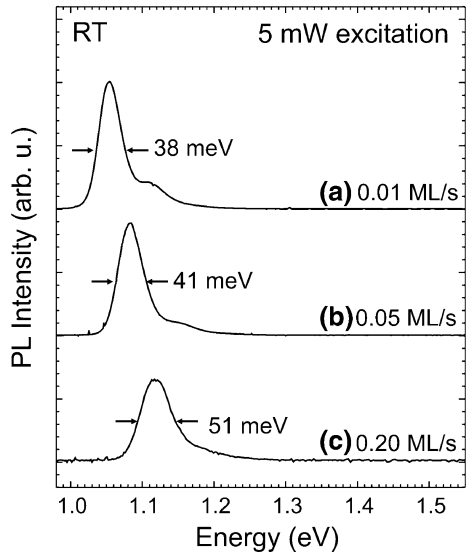

Fig. 4 Room temperature PL spectra of 1.8 ML InAs QDs grown at different InAs growth rates of (**a**) 0.01 ML/s, (**b**) 0.05 ML/s, and (**c**) 0.20 ML/s

QDs grown at 500 °C and overgrown by GaAs at lower overgrowth temperature (460 °C). We observe that the PL spectra are significantly narrower and red shift compared to QDs overgrown at 500 °C (Fig. 4). This observation can be attributed to the suppression of In-Ga intermixing. Moreover, the low temperature growth is expected to preserve the shape of buried QDs [23, 24].

Since *all* QDs experience an evolution in size, shape and composition during overgrowth, the overgrowth process can induce another degree of inhomogeniety. By limiting this evolution the homogeneity of the buried QDs would improve. It is worth to note that the composition inhomogeniety induced by In-Ga intermixing as well as the QD size and shape evolution during the overgrowth process can also be hindered by using a strain-reducing layer [6, 25].

We performed a systematic investigation of the surface morphology evolution during the overgrowth process. Figure 6 shows AFM images of InAs QDs overgrown with GaAs at 460 °C [23]. We observe a drastic collapse of the QD height. At the early stage of GaAs deposition, the covered QDs transform from dome-like shapes to elongated structures along the [1–10] direction. For 3 ML GaAs thickness, the remaining QDs can still be identified in the middle of the mound structures. These mounds have a size of 120–160 nm along the [1–10] direction and 50–70 nm along the [110] direction. The elongation is attributed to the anisotropy of Ga diffusion during growth [26]. Interestingly, after the deposition of 6 ML GaAs, we observed the formation of holes in the middle of the elongated nanostructures. The tiny holes (20–30 nm wide and ~1.5 nm deep) provide evidence of non-preferential GaAs growth on top of the QDs due to strain effects [27].

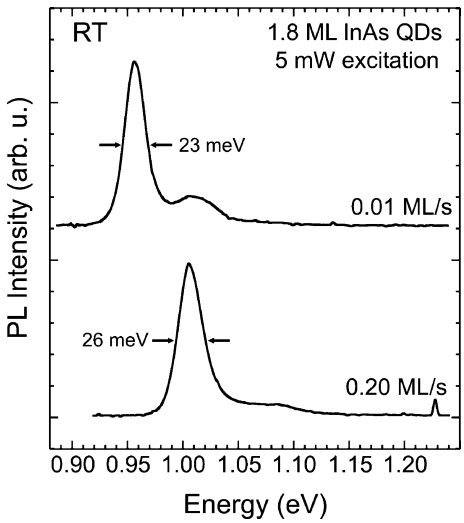

Fig. 5 Room temperature PL spectra of 1.8 ML InAs QD grown at 500 °C with the indicated InAs growth rates and capped with GaAs at a lower growth temperature (460 °C)

Spatial ordering of QDs on the short-range scale: QD molecule formation

Apart from controlling the size and improving the size homogeneity of QDs, there is growing interest to locally control the positioning of QDs. In particular, closely-spaced QDs can act as ''QD molecules'', which are interesting, both as a new playground for studying interacting electronic systems and for their potential application as building blocks of quantum information processing devices [28]. In fact, single QDs can be used as one [29, 30] or two ''qubit'' [31] systems, but cannot be scaled to perform complex operations. For this purpose, chains or groups of QDs are required. A relatively simple way to fabricate *vertical* QD molecules is to grow stacks of QDs [32]. The main disadvantage of this approach is that the composition and strain state of the different layers are usually different and, most importantly, it is hard to envision a controlled tuning of the QD potential profiles, especially of the barrier

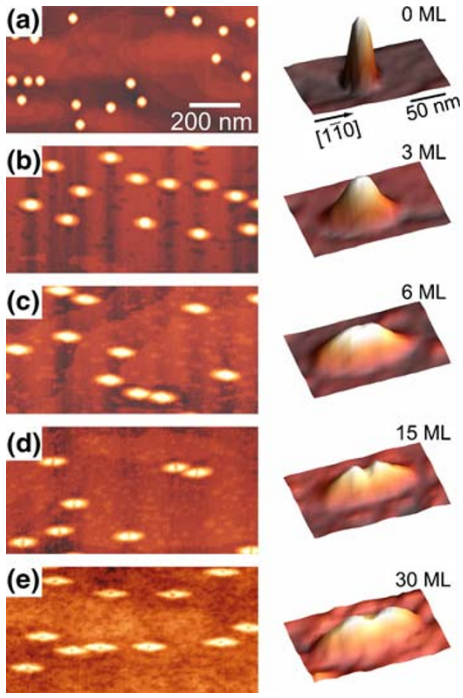

Fig. 6 Surface morphologies of 1.8 ML InAs QDs capped with the indicated amount of GaAs at a lower growth temperature. The panels on the right side show corresponding 3D magnified images of nanostructures on the surface

between them. Therefore, a *lateral* geometry is desirable. Recently, we have reported on a simple route to fabricate lateral QD-molecules, based on the use of *hierarchical* self-assembly. In hierarchically self-assembled structures the result of a self-assembly step is used as the starting point for the subsequent step. Here, the starting point is represented by InAs/GaAs(001) QDs. QDs are buried with a thin GaAs layer and then an in situ etching step is applied. $AsBr_3$ gas is used as etchant. The strain modulation from the buried InAs QDs increases the etching rate of GaAs [33], leading to the spontaneous formation of holes on the GaAs overgrowth surface [33, 34].

The process of nanohole fabrication is illustrated in Fig. 7. An AFM image of the surface morphology of InAs QDs capped with 10-nm GaAs is shown in Fig. 7a. When the etching step is applied, the hole depth and width increase (Fig. 7b–d) with increasing nominal etching depth. (The nominal etching depth is defined as the amount of material removed from an unstrained GaAs(001) substrate under the same etching conditions). The size of these self-assembled nanoholes can be manipulated by changing the etching times. The 5-nm nominal etched nanoholes (Fig. 7d), with an average depth of about 6 nm, are used as a template to fabricate groups of closely spaced InAs QDs (QD molecules).

Figure 8a shows an ensemble of lateral QD bi-molecules (QDBM), obtained by overgrowing the self-assembled nanohole with 2.5 ML InAs at 500 °C. The QDBMs are rather homogeneous in size and the number of isolated QDs can be reduced by growing the nanohole template on a slightly rough surface [35]. Moreover, QDBMs are aligned along the [1–10] direction possibly because of the anisotropic hole shape and anisotropic In diffusion [36]. The number of QDs per QD-molecule can be tuned [37, 38] to a certain extent by changing the InAs growth conditions (Fig. 8b–d). For instance, QD-quad- and hexa- molecules can be obtained by depositing 2.0 ML InAs and 1.8 ML InAs at 450 °C on the nanohole template. For a statistical analysis we select different samples grown under growth conditions, where the percentage of a certain *n*-fold QD molecule is particularly high. For 2.5 ML InAs deposition at 500 °C, we obtain 59% bi-molecules and 40% isolated dots, while for 2 ML InAs deposition at 470 °C, we obtain 52% quad-molecules, 28% tri-molecules, 4% bimolecules, and 16% others. In the case of 1.8-ML InAs deposition at 450 °C, we obtained 32% hexa-molecules, 22% penta-molecules, 8% hepta-molecules and 38% others. We observe that the maximum percentage of *n*-fold QD molecules decreases with increasing *n* (see Fig. 9). *n*-fold QD molecules with large *n* tend to form when the InAs growth is performed at lower substrate temperature, because In adatoms have a higher probability to nucleate new islands before possibly being incorporated into existing QD molecules. We note that the formation of QD molecules with even multiplicity tend to have a higher probability than that of QD molecules with odd *n*. We attribute this effect to the two-fold symmetry of the hole structure.

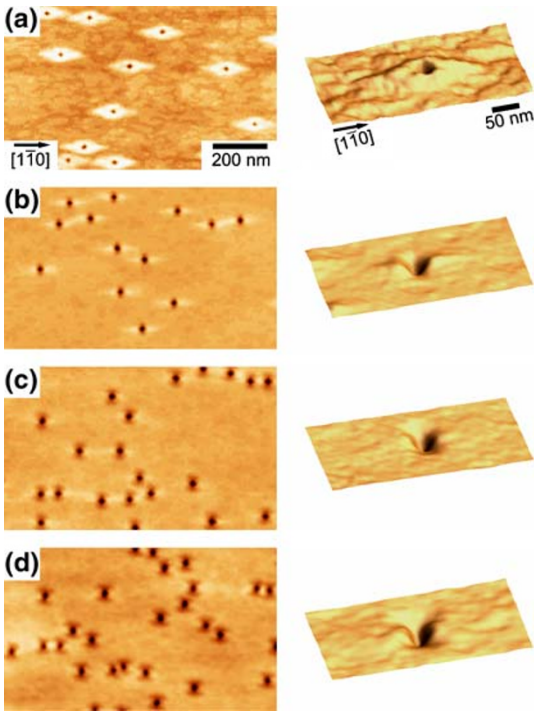

Fig. 7 Surface morphology of 1.8 ML InAs QDs capped with 10-nm GaAs and etched with $AsBr_3$ in situ etching gas for (**a**) 0 nm, (**b**) 1 nm, (**c**) 3 nm, and (**d**) 5 nm nominal etching depth. The panels on the right side show corresponding 3D magnified images of nanostructures on the surface

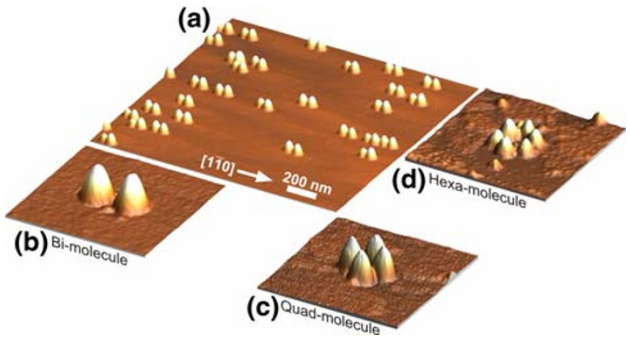

Fig. 8 3D view AFM images of (**a**) QDBM ensemble, (**b**) a single QDBM, (**c**) a single QD quad-molecule, and (**d**) a QD hexa-molecule

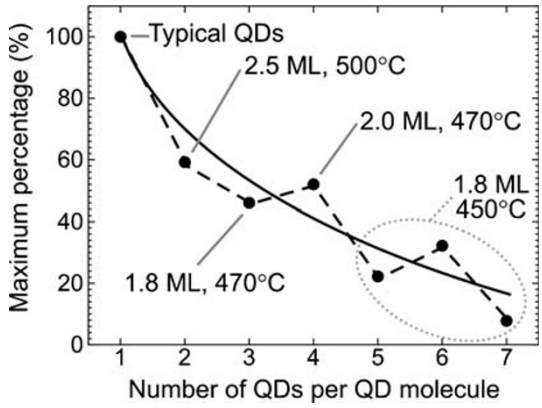

Fig. 9 Maximum percentage of dominant QD molecules as a function of the number of QDs per QD molecule

In order to gather insight into the formation mechanism and into the optical properties of QDBMs, we performed AFM and PL spectroscopy investigations. The samples for this study consisted of nanoholes overgrown with different amounts of InAs. Fig. 10a shows representative AFM images illustrating the hole-filling process. (The 5-nm etched and 2.5 ML InAs filled hole structures are shown in Figs. 7d and 8a, respectively.) From the AFM data, we observe that the hole is still preserved after overgrowth with 0.2 ML InAs. QDBMs start to form at an InAs coverage between 1.6 and 2.0 ML and then they evolve into fully developed QDBMs at a coverage of 2.5 ML. For the PL investigations the InAs layer was overgrown with a thick GaAs layer. For the nanoholes obtained by 5-nm nominal etching depth, the wetting layer (WL) signal at 1.414 eV is the dominant peak, indicating that the underlying QDs are completely removed and only the WL remains. At 0.2 ML InAs deposition, we observe another peak, which is attributed to the second InAs layer that partially fills the etched holes. For 1.6 ML InAs deposition, a third peak appears at smaller energies, which is appointed to the initial stage of the QDBM formation. The linewidth of the peak is 29 meV, indicating a good size uniformity of the QDBMs. Figure 10c contains a summary of the PL peak position at room temperature as a function of deposited amount of InAs. The WL signal is the dominant peak up to 1.6 ML InAs deposition and then the peak from the QDs in the second layer can be observed. It is noteworthy that for 2.5 ML InAs deposition, the QDBMs emit at 0.972 eV, have a linewidth of 30 meV (see inset of Fig. 10c), and the PL intensity is comparable to the original QD layer, which underlines a good size uniformity of the structure and the high crystal quality of the samples, respectively.

While short-range spatial ordering can be achieved by combining several self-assembly steps, it is hard to envision spontaneous long-range ordering of QDs required to address single QDs. The most promising strategy to achieve this goal is to combine the bottom-up approach with the top-down as discussed in the next section.

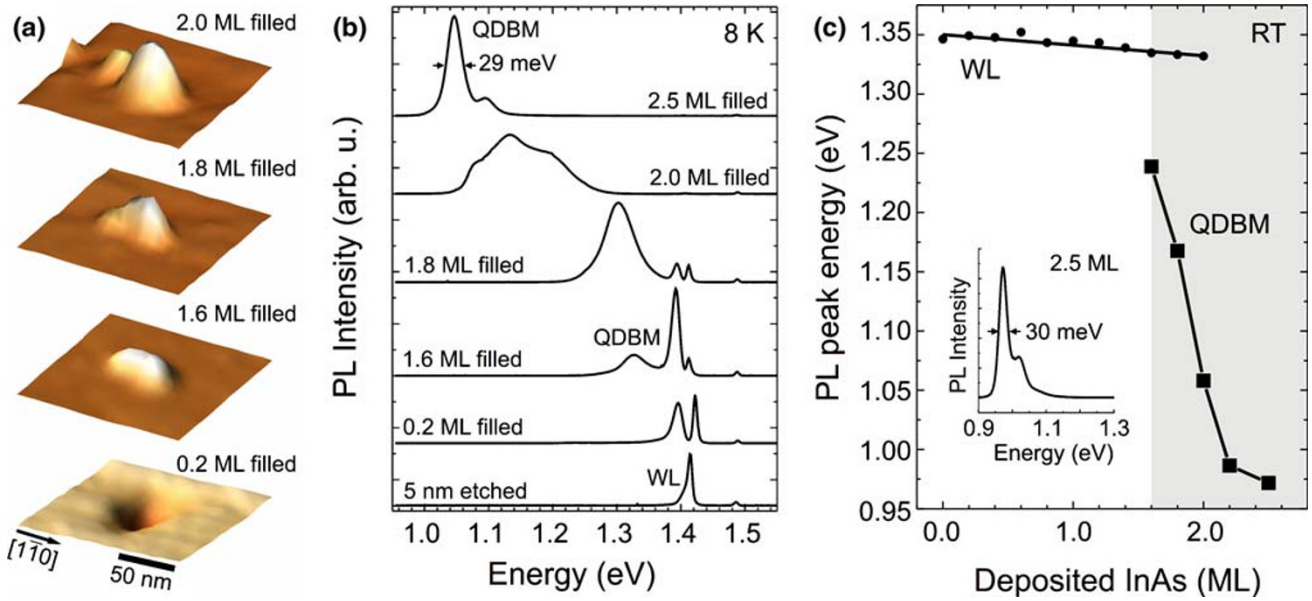

Fig. 10 (**a**) 3D view AFM images of surface structures obtained by overgrowing nanoholes with 0.2 ML, 1.6 ML, 1.8 ML and 2.0 ML InAs. (**b**) Low-temperature PL spectra of the structures developed during the QDBM fabrication process. (**c**) Observed room-temperature PL peak energy versus amount of deposited InAs to fill the nanoholes. Inset in (**b**) shows a room temperature spectrum obtained from the QDBM grown by depositing 2.5 ML InAs on the surface with self-assembled holes

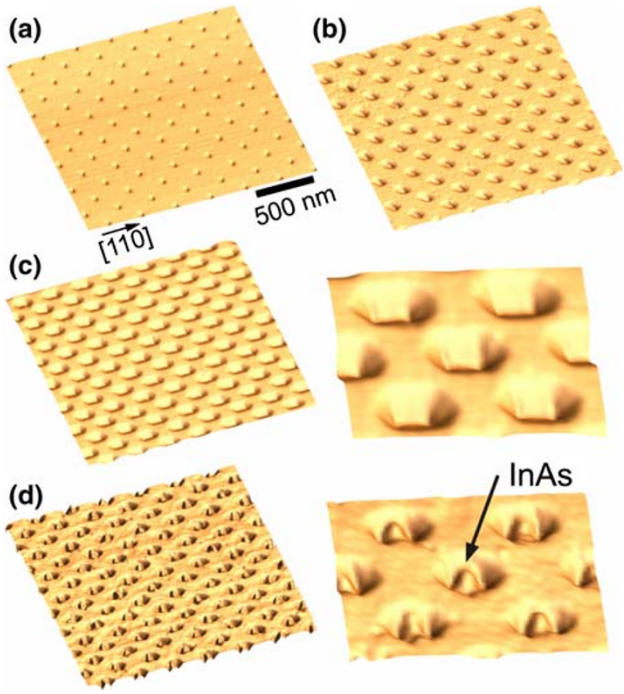

Fig. 11 3D view AFM images of (**a**) initial patterned hole surface, patterned hole surface overgrown with (**b**) 18 ML and (**c**) 36 ML GaAs buffer layer and (**d**) patterned hole surface after 18 ML GaAs buffer layer growth and 2 ML InAs. On the right side of (**c**) and (**d**) magnified images are shown

Spatial ordering of QDs on the long-range scale: Quantum dot crystals

As shown in the previous section, the positioning of self-assembled QDs can be well controlled on a short length scale. In this section, we present a successful method to position self-assembled QDs on the long-range scale by the growth of InAs on patterned substrates. The patterned substrates were prepared by standard electron-beam lithography and reactive ion etching using $SiCl_4$. Details of the pattern preparation have been reported elsewhere [39]. Figure 11a shows a 3D AFM image of a patterned hole surface aligned along [100] and [010] directions. The molecular beam epitaxial growth is performed on this patterned surface. After deposition of an 18 ML GaAs buffer, an enlargement of the hole diameter and a reduction of the hole depth are observed (Fig. 11b). When the deposition proceeds further the holes become facetted (Fig. 11c) [40]. Using these nanoholes as a template for the InAs growth, we can obtain QDs in the patterned holes as shown in Fig. 11d.

Homogeneous and ordered QD arrays can be fabricated by overgrowing the QDs in the patterned holes (Fig. 11d) with a Ga(Al)As capping layer followed by a second InAs QD layer. Figure 12a shows AFM images of a QD array on a flat surface obtained by this procedure. The patterns in this case have 160-nm periodicity. Typically, long-range ordering is observed on the sample. Figure 12b shows a large-scale AFM image ($8 \times 10\ \mu m^2$) which contains *no* QD defects (QD vacancies or QD interstitial defects). From the analysis of height and diameter of each QD in this array, we obtain an average QD height (diameter) of 14.7 nm (67 nm). Remarkably, a narrow size distribution of about 5% is observed (Fig. 12c) [41]. Such a narrow size distribution implies an improvement of the QD size homogeneity due to the pattern.

Once a homogeneous array of QDs is realized, a 3D ordered QD structure, a so-called QD crystal, can be obtained. Figure 13 shows AFM images of the topmost QD layers of 3D QD crystals grown on patterned hole surfaces. The pattern periodicity is 210 nm. This QD crystal is grown under optimized conditions for this pattern periodicity. The first QD layer on the patterned holes is capped with a spacer layer consisting of 8 nm GaAs, 4 nm $Al_{0.4}Ga_{0.6}As$ and 3 nm GaAs. A subsequent 1.8 ML InAs QD layer is grown on top. Repetitive growth of the spacer layer and the QD layer

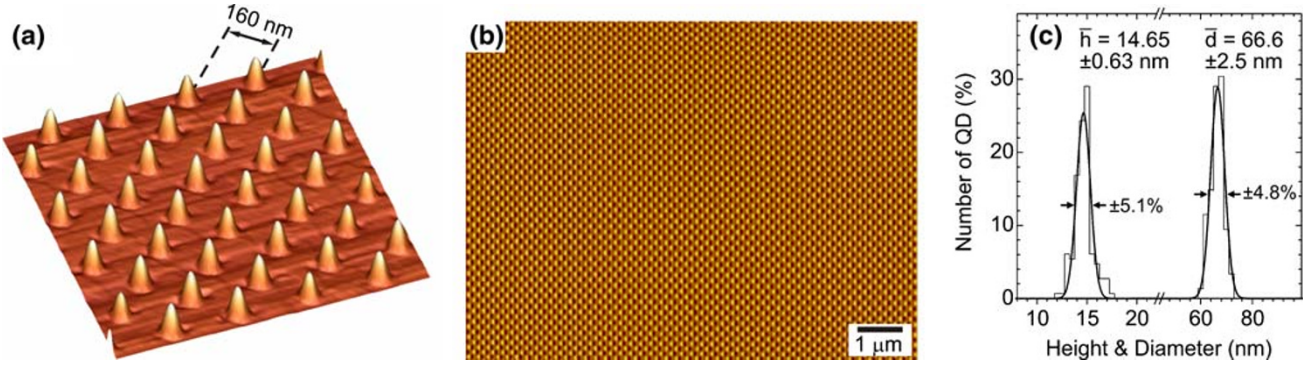

Fig. 12 (**a**) 3D view AFM images of a homogeneous ordered QD array on flat GaAs surface. (**b**) Large area AFM image of the same sample. (**c**) Height and diameter distributions extracted from the AFM image

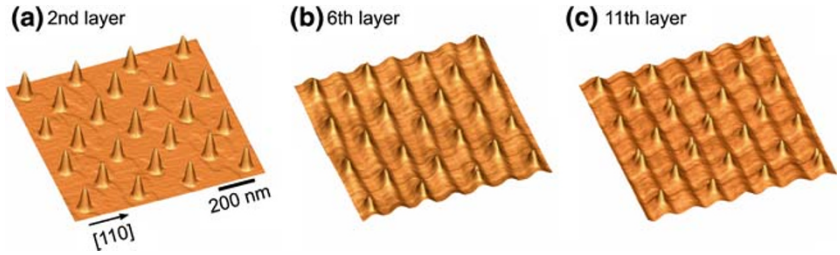

Fig. 13 3D view AFM images of surface QDs in 3D QD crystals containing (**a**) two, (**b**) six, and (**c**) eleven InAs QD layers. The ridge structure developing during the overgrowth of QDs is clearly visible in (**b**) and (**c**)

results in a 3D QD crystal. This is illustrated for six InAs QD layers in Fig. 13b and eleven InAs QD layers in Fig. 13c. Since the strain field from buried QDs predefines the QD formation positions, the number of QD defects (QD vacancies or QD interstitial defects) on the surface is as low as 0.043%. Therefore, we can realize a 3D QD crystal with high structural perfection [39]. As clearly seen in Fig. 13b, the ordered QDs form on top of a ridge structure aligned along [1–10] direction. This ridge, which has a width of ~100 nm and a height of ~3 nm above the flat surface, is caused by an overlap of elongated mound structures that occur during overgrowth of large QDs grown at low growth rate [23]. The height of the surface QDs measured from the top part of the ridge is about 5.6 nm. The small QD size might be due to a redistribution of InAs material in the ridge. The height distribution has a relative width of 10% for the sixth QD layer (Fig. 12b) and 7% for the eleventh QD layer (Fig. 12c).

Interestingly, if we look closer at the shape of surface QDs in the six-fold stacked QD crystal, we observe that some QDs consist of two peaks on top of a common base area. (We call these structures QD pairs). When the number of stacked layers increases to eleven, we observe both well-defined QD pairs and single QDs on the patterned sites. All QD pairs on the surface align along the [1–10] direction. Each QD pair is found at the center of the patterned site. This observation directly implies that the QDs that make up a QD pair form in the vicinity of the buried QD position. The QD pair formation is much less pronounced on the unpatterned surface, where only very few QD pairs have formed in the eleventh layer [42].

Magnified 3D AFM images and lateral peak-to-peak distance as well as base width distributions of QD pairs in the sixth layer are shown in Figs. 14a and b, respectively. An average peak-to-peak distance of 26 nm is observed for this QD layer. A statistical analysis shows that 20% of the patterned sites are occupied by QD pairs. The number of sites occupied by the QD pairs slightly decreases to 16% while the peak-to-peak distance increases to 44 nm for the QD pairs in the eleventh layer (Fig. 14d). This result implies that the stacking of QD pairs can also lead to single QDs in the subsequent layers as has been reported for random QD arrays [32]. For the QDs on the unpatterned surface (not shown), we count only 3% of QD pairs.

In order to account for our experimental observation, we perform kinetic Monte-Carlo (KMC) simulations to investigate the preferential nucleation sites of

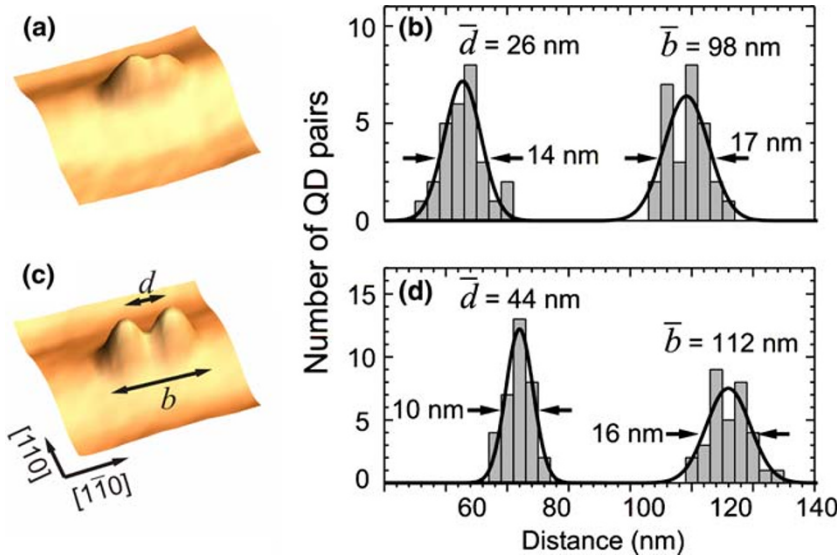

Fig. 14 (**a**) 3D view of a QD pair on the surface of a QD crystal with 6 QD layers. (**b**) Statistical data obtained from QD pairs observed in the same sample. (**c**) 3D view of a QD pair on the surface of a QD crystal with 11 QD layers and (**d**) data for QD pairs observed in the QDC_{11}. Definitions of base width *b* and peak-to-peak distance *d* are shown in (**c**)

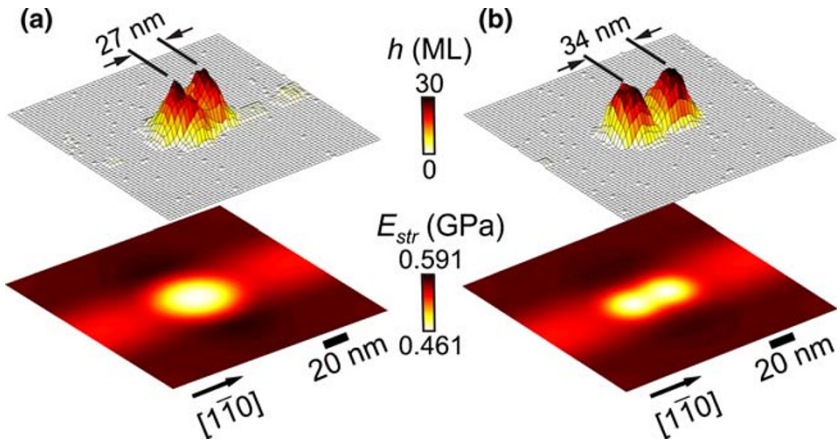

Fig. 15 (**a**) Results of the KMC simulation of the initial QD pair formation on a strain modulated surface. The strain field, which is used as an input in the simulation, is shown below the simulation results. (**b**) The simulation result demonstrating the development of QD pair after its formation (see text)

2D islands on a strain modulated surface. Simulation details are reported in Ref. [42]. Figure 15 shows the calculated surface strain energy profile and the results of the KMC simulations. In Fig. 15a, we observe only one strain energy minimum positioned on top of the buried QD. Consequently, almost 70% of all simulations result in single elongated 2D islands that form on top of the strain minima positions. Our simulations also produce 30% of double 2D islands aligned along [1–10] that form in the vicinity of the strain energy minima. The formation of double 2D islands aligned along the ridge orientation can be understood in the following way: In the simulations the diffusion coefficient of an adatom (surface atom without neighboring atoms) is $D \propto (2k_BT/h)\ \exp(E_{str}/k_BT)$, where k_BT is thermal energy and E_{str} is the surface strain energy density. As shown in the bottom part of Fig. 15a, E_{str} along [1–10] is smaller than that along [110], which implies that the diffusion coefficient of adatoms diffusing along [1–10] is smaller than along [110]. Hence, atoms preferably aggregate on the ridge in the vicinity of the strain energy minimum positions, where they nucleate into stable 2D islands. In our simulation the average center-of-mass distance between double 2D islands is 27 nm, which is in excellent agreement with the 26 nm average peak-to-peak QD distance obtained from our experiment. Furthermore, the simulated 30% of double 2D islands compares reasonably well with the 20% QD pairs found in our experiment.

In Fig. 15b, we show the calculated surface strain energy obtained from the buried QD pair in the sixth layer using the peak-to-peak distance and the corresponding ridge structure deduced from the AFM images. In this case, we find two strain energy minima on top of each buried QD of the QD pair. The simulation in Fig. 15b produces 93% double 2D islands, and the average center-of-mass distance between the double 2D islands increases to 34 nm. This simulation results allow us to conclude that QD pairs become more separated in subsequent layers, which is in good agreement with our experimental observations.

Conclusion

In conclusion, ordering of self-assembled InAs/GaAs(001) QDs on a multi-length scale was discussed. Beginning with the study of the QD morphology, we observed dome and pyramid shaped InAs QDs on GaAs surface. The next step is the ordering of QD size. By varying the growth rate, we can improve the QD size homogeneity, while the homogeneity of the QD size distribution in the GaAs matrix can be further improved by overgrowth at lower growth temperature. The morphology of nanostructures on the surface developing during GaAs overgrowth was also investigated. By using an atomic-layer precise in situ etching, we have realized self-assembled nanoholes, which can be used as a template for fabricating QD molecules. Ordering of the QD position on a long-range scale is obtained by the growth on patterned substrates. The ordered QD arrays show remarkable size homogeneity. Finally, we reported on the phenomenon of lateral QD replication during stacking of self-assembled QDs to fabricate 3D QD crystals.

Acknowledgments The technical support of U. Waizmann, T. Reindl, and M. Riek is acknowledged. The authors would like to thank K. von Klitzing for continuous interest and support. This work was financially supported by the Bundesministerium für Bildung und Forschung (contract number: 03N8711).

References

1. D. Bimberg, M. Grundmann, N.N. Ledentsov, *Quantum Dot Heterostructures* (Wiley, Chichester, 1999)

2. Y. Masumoto, T. Takagahara, *Semiconductor Quantum Dots: Physics, Spectroscopy and Applications* (Springer, Berlin Heidelberg 2002)
3. J.M. Gérard, B. Sermage, B. Gayral, B. Legrand, E. Costard, V. Thierry-Mieg, Phys. Rev. Lett. **81**, 1110 (1998)
4. T. Yoshie, A. Scherer, J. Hendrickson, G. Khitrova, H.M. Gibbs, G. Rupper, C. Ell, O.B. Shchekin, D.G. Deppe, Nature **432**, 2000 (2004)
5. M. Sugawara, *Semiconductors and Semimetals*, vol. 60, ed. by R.K. Willardson, A.C. Beer (Academic Press, London 1999)
6. O.G. Schmidt, S. Kiravittaya, Y. Nakamura, H. Heidemeyer, R. Songmuang, C. Müller, N.Y. Jin-Phillipp, K. Eberl, H. Wawra, S. Christiansen, H. Gräbeldinger, H. Schweizer, Surf. Sci. **514**, 10 (2002)
7. V.A. Shchukin, D. Bimberg, Rev. Mod. Phy. **71**, 1125 (1999)
8. J. Stangl, V. Holý, G. Bauer, Rev. Mod. Phys. **76**, 725 (2004)
9. J. Márquez, L. Geelhaar, K. Jacobi, Appl. Phys. Lett. **78**, 2309 (2001)
10. T. Kaizu, K. Yamaguchi, Jpn. J. Appl. Phys. **42**, 4166 (2003)
11. S. Ruvimov, P. Werner, K. Scheerschmidt, U. Gösele, J. Heydenreich, U. Richter, N.N. Ledentsov, M. Grundmann, D. Bimberg, V.M. Ustinov, A.Y. Egorov, P.S. Kop'ev, Zh.I. Alferov, Phys. Rev. B **51**, 14766 (1995)
12. G. Costantini, C. Manzano, R. Songmuang, O.G. Schmidt, K. Kern, Appl. Phys. Lett. **82**, 3194 (2003)
13. G. Costantini, A. Rastelli, C. Manzano, R. Songmuang, O.G. Schmidt, K. Kern, H. von Känel, Appl. Phys. Lett. **85**, 5673 (2004)
14. G. Costantini, A. Rastelli, C. Manzano, P. Acosta-Diaz, G. Katsaros, R. Songmuang, O.G. Schmidt, H. von Känel, K. Kern, J. Cryst. Growth **278**, 38 (2005)
15. A. Rastelli, H. von Känel, Surf. Sci. 532–535, 769 (2003).
16. I. Mukhametzhanov, Z. Wei, R. Heitz, A. Madhukar, Appl. Phys. Lett. **75**, 85 (1999).
17. G. Medeiros-Ribeiro, A.M. Bratkovski, T.I. Kamins, D.A.A. Ohlberg, R.S. Williams, Science **279**, 353 (1998)
18. D. Leonard, M. Krishnamurthy, C.M. Reaves, S.P. Denbaars, P.M. Petroff, Appl. Phys. Lett. **63**, 3203 (1993)
19. R. Songmuang, S. Kiravittaya, M. Sawadsaringkarn, S. Panyakeow, O.G. Schmidt, J. Cryst. Growth **251**, 166 (2003)
20. Y. Nakata, K. Mukai, M. Sugawara, K. Ohtsubo, H. Ishikawa, N. Yokoyama, J. Cryst. Growth **208**, 93 (2000)
21. Y. Chen, J. Washburn, Phys. Rev. Lett. **77**, 4046 (1996)
22. S. Kiravittaya, Y. Nakamura, O.G. Schmidt, Physica E **13**, 224 (2002)
23. R. Songmuang, S. Kiravittaya, O.G. Schmidt, J. Cryst. Growth **249**, 416 (2003)
24. A. Rastelli, E. Müller, H. von Känel, Appl. Phys. Lett. **80**, 1438 (2002)
25. K. Nishi, H. Saito, S. Sugou, J.-S. Lee, Appl. Phys. Lett. **74**, 1111 (1999)
26. K. Shiraishi, Appl. Phys. Lett. **60**, 1363 (1992)
27. Q. Xie, P. Chen, A. Madhukar, Appl. Phys. Lett. **65**, 2051 (1994).
28. G. Burkard, G. Seelig, D. Loss, Phys. Rev. B **62**, 1581 (2000)
29. T.H. Stievater, X. Li, D.G. Steel, D. Gammon, D.S. Katzer, D. Park, C. Piermarocchi, L.J. Sham, Phys. Rev. Lett. **87**, 133603 (2001)
30. A. Zrenner, E. Beham, S. Stufler, F. Findeis, M. Bichler, G. Abstreiter, Nature **418**, 612 (2002)
31. X. Li, Y. Wu, D. Steel, D. Gammon, T.H. Stievater, D.S. Katzer, D. Park, C. Piermarocchi, L.J. Sham, Science **301**, 809 (2003)
32. Q. Xie, A. Madhukar, P. Chen, N.P. Kobayashi, Phys. Rev. Lett. **75**, 2542 (1995)
33. H. Schuler, N.Y. Jin-Phillipp, F. Phillipp, K. Eberl, Semicond. Sci. Technol. **13**, 1341 (1998)
34. S. Kiravittaya, R. Songmuang, O.G. Schmidt, J. Cryst. Growth **251**, 258 (2003)
35. L. Wang, A. Rastelli, S. Kiravittaya, R. Songmuang, O.G. Schmidt, B. Krause, T.H. Metzger, Nanoscale Res. Lett. (in press)
36. E. Penev, S. Stojković, P. Kratzer, M. Scheffler, Phys. Rev. B **69**, 115335 (2004)
37. O.G. Schmidt, Ch. Deneke, S. Kiravittaya, R. Songmuang, H. Heidemeyer, Y. Nakamura, R. Zapf-Gottwick, C. Müller, N.Y. Jin-Phillipp, IEEE J. Sel. Top. Quantum Electron. **8**, 1025 (2002)
38. R. Songmuang, S. Kiravittaya, O.G. Schmidt, Appl. Phys. Lett. **82**, 2892 (2003)
39. S. Kiravittya, H. Heidemeyer, O.G. Schmidt, Physica E **23**, 253 (2004)
40. H. Heidemeyer, C. Müller, O.G. Schmidt, J. Cryst. Growth **261**, 444 (2004)
41. S. Kiravittaya, O.G. Schmidt, Appl. Phys. Lett. **86**, 206101 (2005)
42. S. Kiravittaya, H. Heidemeyer, O.G. Schmidt, Appl. Phys. Lett. **86**, 263113 (2005)